20th Australasian Fluid Mechanics Conference
Perth, Australia
5-8 December 2016

# Steady and unsteady loads acting on a hydrofoil immersed in a turbulent boundary layer

**S. M. Smith[1], B. W. Pearce[1], P. A. Brandner[1], D. B. Clarke[2], D. J. Moreau[3] and Y. Xue[1]**

[1]Australian Maritime College
University of Tasmania, Launceston, Tasmania 7250, Australia
[2] Maritime Division
Defence Science and Technology Group, Fishermans Bend, Victoria 3207, Australia
[3]School of Mechanical and Manufacturing Engineering
University of New South Wales, Sydney, New South Wales 2052, Australia

## Abstract

This study investigated steady and unsteady loads acting on a hydrofoil immersed in a turbulent boundary layer. Measurements were performed in a cavitation tunnel in which the hydrofoil was mounted spanwise normal from the test section ceiling, via a 6-component force balance. The turbulent boundary layer was artificially thickened via an array of transverse jets located upstream of the test section. The effect of boundary layer thickness was investigated, in which various thicknesses were generated to allow partial or full immersion of two hydrofoils, each with different aspect ratios. The effect of varying incidence and Reynolds number on the hydrodynamic loading was also investigated. Steady forces were found to be significantly affected by the scale of the boundary layer, particularly in the stall region. Identification of a broad peak in the unsteady force spectra, was made at a constant reduced frequency of 0.2. The peak was dependent on boundary layer thickness and Reynolds number. Furthermore, a low frequency stall component, superimposed over the existing broadband excitation of the boundary layer turbulence, was apparent in the spectra past stall.

## Introduction

Control surfaces for marine vessels are typically located at the stern, where the boundary layer has had the full vessel length to develop and thicken. As control surfaces are generally compact compared to overall length scales, they are at least partially immersed within the turbulent flow about the vessel stern. In addition, the boundary layer is further thickened or separated due to the adverse pressure gradient generated at the aft end of the vessel [1]. Hence, these control surfaces are subject to unsteady loading and become a source of vibration and noise. To minimise these effects, insight into the flow physics and excitation spectra are required. This would enable more rigorous analysis and design for optimisation of control surface structural response.

Despite extensive development of theoretical models [8] for the prediction of unsteady loads on a lifting surface, there is little experimental data available in literature. Previous investigations have involved aerofoils immersed in grid-generated turbulence with lift spectra measured directly or derived from surface pressure measurements [6, 7]. Although valuable for providing insight into associated phenomena, these results cannot be directly transferred to the structured wall bounded turbulent flow of a boundary layer.

This preliminary work aims to provide insights into the physics determining the loading of a hydrofoil encountering the structured turbulence of an oncoming boundary layer. Forces, both steady and unsteady, were obtained for a range of Reynolds numbers (*Re*), incidence ($\alpha$) and boundary layer thicknesses ($\delta$). Immersion of the hydrofoil span in the boundary layer was adjusted from about $^1/_8$ to the full span. Partial results were gained from a previous investigation [5] with the current work expanding from it where a greater range of parameters were examined, in particular, a range of $\delta$. These results also provide additional guidance into the frequency response necessary from an improved force balance and model design for future unsteady measurements.

## Experimental Overview

### Model Hydrofoil Details

Hydrofoil geometry has been selected based on the requirements discussed above for the modelling of unsteady conditions typical of those experienced by control surfaces. The chosen geometry was a NACA 0012 profile with a symmetric (unswept) trapezoidal planform with a 80 mm tip and 120 mm root chord. Two models were constructed with spans of 120 mm and 240 mm. This achieved a wide range of oncoming boundary layer thickness to hydrofoil span ratios, from $^1/_8$, up to 1. The chord length was chosen to be compatible with mounting to the water tunnel test section and sufficient to obtain chord-based *Re* values of $1 \times 10^6$.

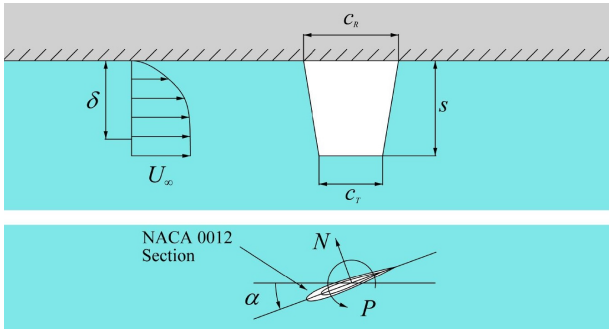


Figure 1: Schematic of the experimental setup whereby a ceiling mounted hydrofoil encounters a turbulent boundary layer that immerses it to varying degrees (top). A bottom view depicting the force balance coordinate system whose origin is located on the root mid-chord is also shown (bottom).

The response spectrum of both hydrofoils was determined from an impact test [5] with results summarized in Table 1. First mode natural frequencies were obtained in air at 536 Hz and 170 Hz, and in water at 273 and 86 Hz for the 120 mm and 240 mm models respectively. The in water values were calculated using an added mass estimate [3]. Both models were machined from solid Aluminium 6061-T6 billets to 0.8 μm surface finish and 0.1 mm surface tolerance. The models were anodised to a thickness of approximately 5μm.

### Experimental Setup

| Hydrofoil Dynamic Properties | Hydrofoil span | |
|---|---|---|
| | 120 mm | 240 mm |
| First bending mode in air (Hz) | 536 | 170 |
| First bending mode in water (Hz) | 273 | 86 |
| Second bending mode in air (Hz) | - | 783 |
| Second bending mode in water (Hz) | - | 399 |
| Added mass for first and second bending modes, $2m_a$(kg) | 0.94 | 1.88 |
| Mass of hydrofoil, $m$ (kg) | 0.33 | 0.60 |

Table 1: Natural frequencies, mass and added mass values of the model hydrofoils utilized in the experiment [3].

Measurements were carried out in the Cavitation Research Laboratory (CRL) water tunnel at the Australian Maritime College. The tunnel test section is 0.6 m square by 2.6 m long in which the operating velocity and pressure ranges are 2 to 12 m/s and 4 to 400 kPa absolute respectively. The tunnel volume is 365m$^3$ with demineralised water (conductivity of order 1$\mu$S/cm). The test section velocity is measured from one of two (high and low range) Siemens Sitransp differential pressure transducers models 7MF4433-1DA02-2AB1-Z and 7MF4433-1FA02-2AB1-Z (measuring the calibrated contraction differential pressure) with estimated precisions of 0.007 and 0.018 m/s respectively. A detailed description of the facility is given in [4].

A schematic representation of the test set-up is given in Figure 1 along with the definition of the coordinate system used and the main geometric parameters. The models were mounted on a 6-component force balance extending vertically into the flow through a 160 mm diameter penetration in the tunnel ceiling. The 160 mm diameter penetration was made fair (to 50$\mu$m) using a disk mounted, in this case, on the measurement side of the balance. The fairing disk has a typical 0.5 mm radial clearance to avoid interference with the force measurement. Of the total load vector measured, steady and unsteady components of normal force and pitching moment are presented. Spanwise forces and roll/yaw moments are not considered as they may be contaminated by the wall pressure distribution acting on the disk with this setup. Data was sampled at 1 kHz for durations sufficient to capture 1 000 and 22 000 chord passages ($= TU_\infty/c$ where $T$ is the acquisition period, $U_\infty$ is the freestream velocity and c is the mean chord) for steady and unsteady measurements respectively.

Measurements were made at a streamwise location 1.9 m downstream from the test section entrance to maximise hydrofoil immersion in the boundary layer. To obtain a test section ceiling boundary layer of the desired scale, it was artificially thickened via an array of cross flow jets located upstream of the test section. At the test location, $\delta$ was adjusted from its natural state of 33 mm, through to a maximum of 99 mm. $\delta$ was controlled by adjustment of the flow rate through the jet array. A detailed description and performance characteristics of the CRL boundary layer manipulator is given in [2]. Based on the performance of the plate geometries previously tested for boundary layer thickening, "Plate E" (68 $\times$ 10 mm holes triangularly spaced over 4 rows) was chosen for the present investigation. This was based on the resulting mean velocity profile of the artificial thickened boundary layer comparing most favourably with the natural profile, particularly in the outer (or wake) region [2]. This is important as the outer region is the largest portion of the boundary layer and is therefore seen as the most significant contributor to the production of unsteady forces.

The force balance was calibrated by a least squares fit between a basis vector loading cycle and the 6 outputs giving a $6 \times 6$ matrix. An estimated precision on all components is less than 0.1%. Forces were measured at mean chord-based $Re$ values (mean chord, $c = (c_T + c_R)/2 = 0.1$m), of 0.2, 0.4, 0.6, 0.8 and $1.0 \times 10^6$. Each $Re$ was run for a range of $\alpha$, from $-1°$ to beyond stall at 25° and 20° for the 120 mm and 240 mm span hydrofoils respectively. $\alpha$ is adjusted using the balance automated indexing system incremented in 0.5° steps with an incremental precision less than 0.001°. The tunnel was pressurised up to 350 kPa to minimize cavitation occurrence.

### Results

The measured normal force, $N$, and pitching moment, $P$, are presented as dimensionless coefficients, $C_N = 2N/(\rho U_\infty^2 A)$ and $C_P = 2P/(\rho U_\infty^2 Ac)$, respectively. $U_\infty$ denotes the freestream velocity, $\rho$ is the liquid density and $A$ is the planform area. $\delta$ is where the boundary layer velocity, $U$, becomes equal to $0.99U_\infty$. Unsteady loads are presented using power spectral density (PSD) in a narrowband format with a frequency resolution of 1 Hz. Spectra have been calculated using Welchs averaged modified periodogram method of spectral estimation with a Hammimg window function and 50% overlap. The 95% confidence interval on the narrow band auto spectral density is $-0.3690/+0.3857$ N$^2$dB/Hz.

#### Steady Forces

Steady normal force and pitching moment coefficients for the thickest boundary layer ($\delta$ = 99 mm) at incremental $Re$ are presented in Figure 2. The 240 mm span model exhibits an increased $C_N$ slope ($\partial C_N/\partial\alpha$) and maximum $C_N$, as well as an earlier stall incidence. For both geometries, the $\alpha$ at which stall occurs increases with $Re$ by about 6°.

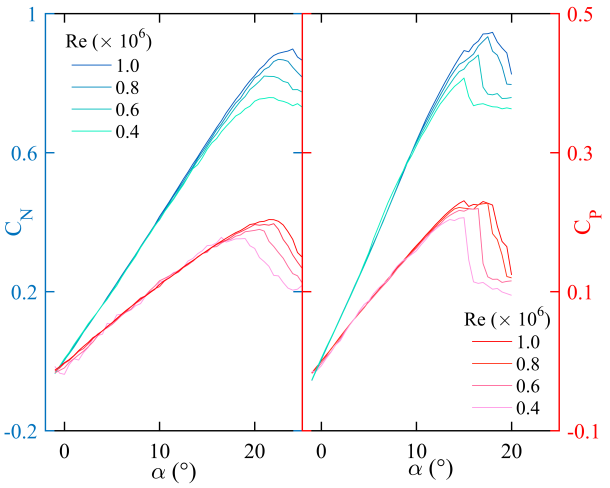


Figure 2: Normal force and pitching moment coefficients with incidence for 120 mm span (left) and 240 mm span (right) hydrofoil models. They were immersed in a turbulent boundary layer with $\delta = 99$ mm, for $Re$ between $0.4 \times 10^6$ and $1.0 \times 10^6$.

A comparison of the normal force measured for the 120 mm span hydrofoil for 3 boundary layer thicknesses is presented in Figure 3. $\partial C_N/\partial\alpha$ is seen to decrease with an increase in $\delta$ as the hydrofoil becomes increasingly immersed in the lower velocity flow of the boundary layer. Initially, the effect is quite gradual with stall delayed by 1.5° as the foil submergence is increased, from about $^1/_3$, to $^1/_2$ of the span. This corresponds with an increase in maximum $C_N$ of less than 1%. Increasing $\delta$ further to 99 mm (nominally fully immersing the hydrofoil within the boundary layer) sees a significant drop in max $C_N$ to 0.868, along with a small decrease in stall angle. Notably in this condition, there is a significant change from a sudden, leading-

edge type, to a gradual, trailing-edge type, stall behaviour. This suggests that the boundary layer is having significant impact on the state of flow over the hydrofoil. The level of unsteadiness is presented using RMS of the steady measurements ($C'_N$), shown in Figure 3. The $C'_N$ reveals a trend of increased fluctuation with boundary layer thickness for all pre-stall α. The significant increase in the $C'_N$ with α in each condition, coincides with the onset of stall.

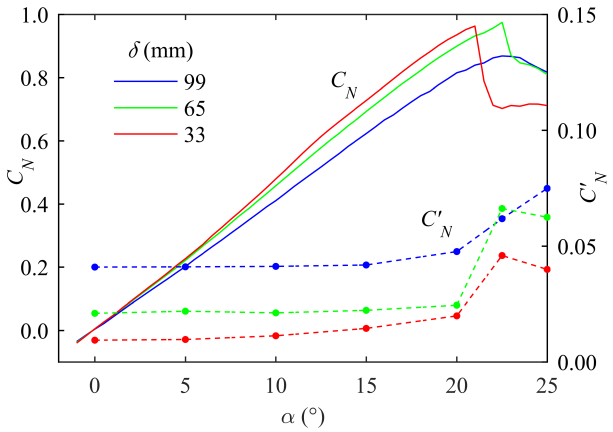


Figure 3: $C_N$ and $C'_N$ values with α for 120 mm hydrofoil model with $Re = 0.8 \times 10^6$ for several δ (All RMS results are derived from unsteady measurements except $\alpha = 5°, 10°, 20°$ and 25° for δ = 65 mm). Pre-stall normal forces are dependent on δ with higher RMS values for larger δ. Stall is delayed as δ increases with stall characteristics shifting from a sudden drop-off to a smooth transition.

## Unsteady Forces

To allow characteristic properties to be identified, spectra have been obtained from time series of the normal force and presented non-dimensionally in the form of the power spectral density (PSD), with the excitation frequency ($f$) represented as reduced frequency ($f' = fc/U_\infty$). Due to space limitations, only results of the 120 mm span hydrofoil are presented. Peak frequencies are present in all spectra due to the frequency response of both the force balance and hydrofoil. Identified in a previous study [5], the first and second natural frequencies of the force balance is observed in Figure 4 to be around 150 and 180 Hz. The peak at around 310 Hz is attributable to the hydrofoil first mode natural frequency, close to the estimate of 273 Hz given in Table 1. Error in the estimation is potentially due to the simplification to a rectangular plate and a low aspect ratio planform being more susceptible to 3D effects. The additional peaks at 350 and 450 Hz is attributed to power line odd harmonics. Due to this inherent dynamic response from the coupled balance/hydrofoil system, the resolvable frequency range for the present measurements only extends out to about 100 Hz. This equates to a $f'$ from 0.9 to 4.5 for $Re$ of $1.0 \times 10^6$ and $0.2 \times 10^6$ respectively. An improved force balance and hydrofoil design, both resulting with increased natural frequencies, are being considered for a follow-on experimental campaign to extend the resolvable frequency range out to about 1 kHz.

Figure 5 shows the effect of $Re$ on the PSD of $C_N$ at $\alpha = 0°, 15°$ and 22.5° for the 120 mm span hydrofoil in a δ = 99 mm. In the lower frequency range ($f' < 0.3$), there is an increase in power with α for all $Re$. At $\alpha = 0°$ and 15°, the order of Re is sequential, with higher $Re$ exhibiting greater power at $f' < 1$. This tendency does not continue at $\alpha = 22.5°$ with $Re \leq 0.8 \times 10^6$ exhibiting a different trend and jumping above higher $Re$ spectra at approximately $0.02 < f' < 0.5$. This suggests a changeover with $Re$ dependency after stall as at $Re \leq 0.8 \times 10^6$, the hydrofoil has stalled. This illustrates the addition of the stall phenomena, exhibiting a low frequency component (i.e. relatively large wake structures), to the existing effect of the boundary layer turbulence on the unsteady forces.

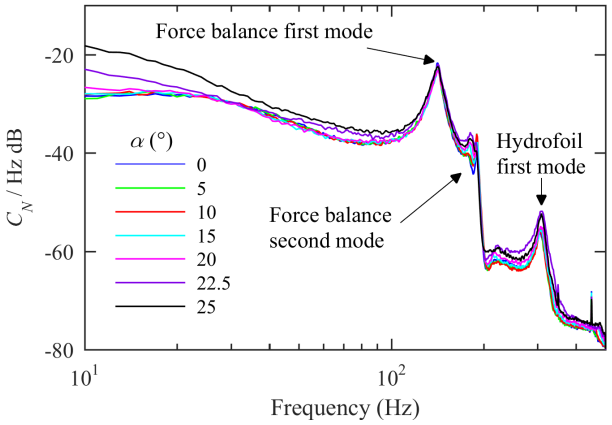


Figure 4: PSD function of $C_N$ for 120 mm span hydrofoil with δ = 99 mm and $Re = 0.8 \times 10^6$ for various α. Contamination caused by the excitation of the force balance and model natural frequencies can easily be seen. The systems inherent dynamic response permits a resolvable frequency range up to approximately 100 Hz.

In Figure 5, a broad peak is clearly observed in all spectra for $\alpha = 0°$ at about $f' = 0.2$. The peak starts to become lost $\alpha = 15°$ with the relative broadband increase in power at $f' < 0.2$ and the peaks magnitude seemingly unaffected by the increased α .This trend continues as the peak becomes even harder to distinguish at $\alpha = 22.5°$. With the peak consistently occurring at approximately $f' = 0.2$, implies that the advection of the flow disturbance causing the unsteady force is about 1/5 of the free-stream advection speed. Furthermore, the peak appears unaffected by α, suggesting it is due to another factor.

The effect of increasing boundary layer thickness on the 120 mm span hydrofoil power spectra at various α is shown in Figure 6. As also seen in Figure 6, for $f' < 1$, there is a broadband power rise with an increase in δ for all α below stall. The broadband peak at $f' \approx 0.2$ discussed previously, is also evident in Figure 6. Furthermore, there is a noticeable increase in the relative amplitude of this peak with increasing δ for pre-stall incidences ($\alpha = 0°$ and 15°). This is attributed to the increased hydrofoil immersion in the boundary layer, resulting in greater exposure to the structured turbulence and therefor, a rise in the unsteady forces. This is in contrast to the steady normal force component decreasing with increasing δ shown in Figure 3.

At $\alpha = 15°$ in Figure 6, a significant rise in power is observed at $f' = 0.02$ for $\delta = 33$ mm and 65 mm, but not for $\delta = 99$ mm. This trait is also evident at $\alpha = 22.5°$ for $\delta = 65$ mm, but not at $\delta = 99$ mm and 33 mm, both of which have stalled. This change in trend at the lowest frequency cannot be attributed to an artefact of the processing method used. At this point, there is also no explanation in terms of the flow physics. This aspect will be further looked at in future more detailed investigations.

## Conclusions

Effects of boundary layer thickness on steady and unsteady loads acting on a hydrofoil were investigated in a water tunnel. Steady forces of a hydrofoil experiencing a thicker bound-

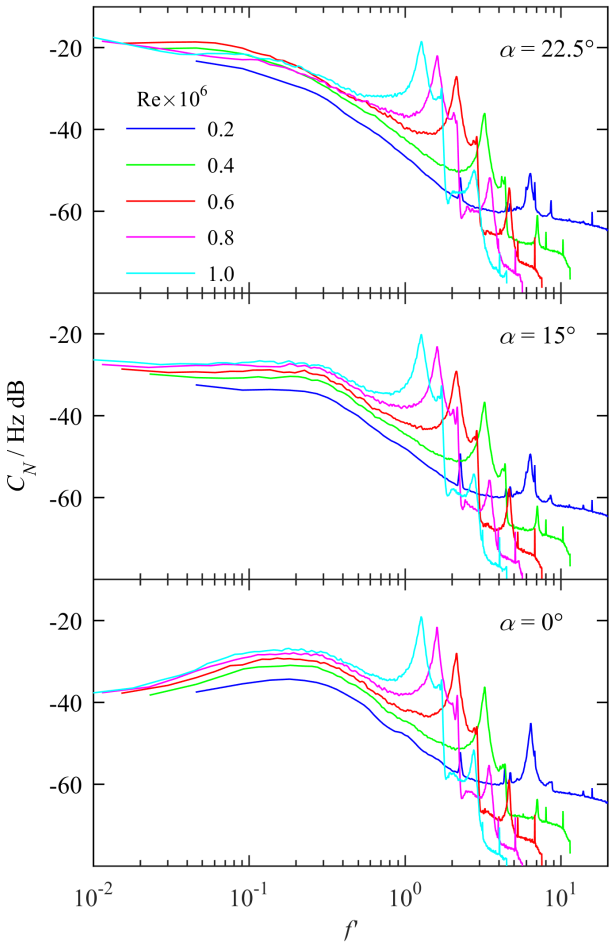


Figure 5: $C_N$ power spectra of the 120 mm span hydrofoil at δ = 99 mm and various *Re* for α = 0° (bottom), 15° (middle) and 22.5° (top).

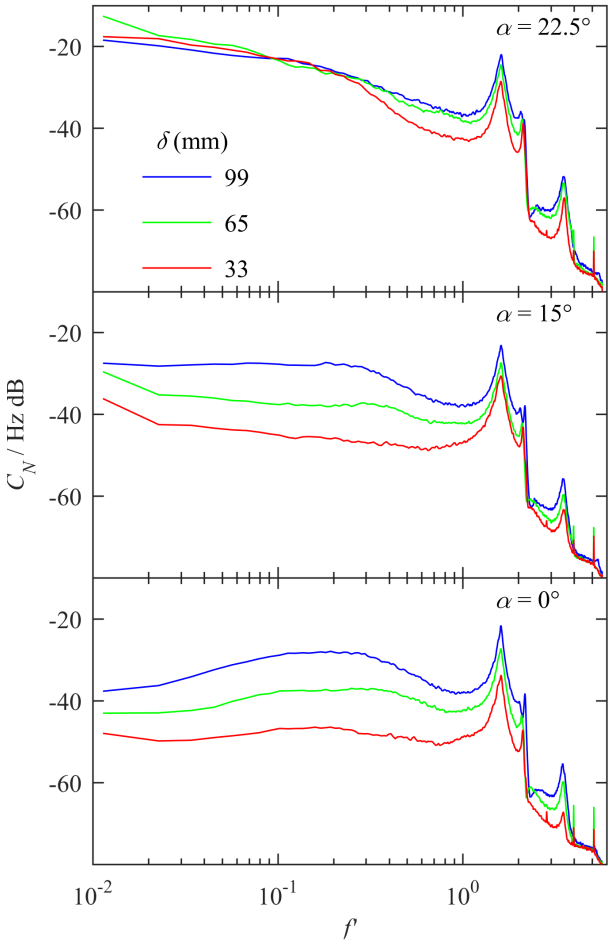


Figure 6: The effect of δ on the relationship between α and $C_N$ spectra of the 120 mm span hydrofoil at $Re = 0.8 \times 10^6$ for α = 0° (bottom), 15° (middle) and 22.5° (top).

ary layer saw reductions in $\partial C_N/\partial\alpha$, changes in stall characteristics and experienced greater unsteadiness. The power spectra revealed the addition of a low frequency stall component (i.e. relatively large wake structures), to the existing effect of the boundary layer turbulence on the hydrofoil unsteady forces. Observations made of the broad peak at a constant reduced frequency of 0.2 imply that the advection of the flow disturbance causing the unsteady force on the hydrofoil is about $^1/_5$ of the free-stream advection speed. The results indicate that an extended frequency range out to about 1 kHz is desired for a future more detailed investigation.


### Acknowledgements

The authors acknowledge the support of the Research Training Centre of Naval Design and Manufacturing (RTCNDM) in this investigation. The RTCNDM is a University-Industry partnership established under the Australian Research Council (ARC) Industry Transformation grant scheme (ARC IC140100003).


### References


[1] Alin, N., Bensow, R. E., Fureby, C., Huuva, T. and Svennberg, U., Current capabilities of des and les for submarines at straight course, *Journal of Ship Research*, **54**, 2010, 184–196.

[2] Belle, A., Brandner, P. A., Pearce, B. W., de Graaf, K. L. and Clarke, D. B., Artificial thickening and thinning of cavitation tunnel boundary layers, *Experimental Thermal and Fluid Science*, **78**, 2016, 75–89.

[3] Blevins, R. D., *Formulas for natural frequency and mode shape*, Van Nostrand Reinhold Co., New York, 1979.

[4] Brandner, P. A., Lecoffre, Y. and Walker, G. J., Design considerations in the development of a modern cavitation tunnel, in *16th Australasian Fluid Mechanics Conference*, 2007, 630–637.

[5] Khoo, M., Brandner, P., Pearce, B., Clarke, D., Butler, D. and Belle, A., An australian capability for submarine control surface performance evaluation, in *Mast Asia Conference 2015*, 1–19.

[6] Lysak, P. D., Capone, D. E. and Jonson, M. L., Unsteady lift of thick airfoils in turbulent flow, in *ASME 2009 International Mechanical Engineering Congress and Exposition*, American Society of Mechanical Engineers, 57–63.

[7] Mish, P. F. and Devenport, W. J., An experimental investigation of unsteady surface pressure on an airfoil in turbulence - Part 1: Effects of mean loading, *Journal of Sound and Vibration*, **296**, 2006, 417–446.

[8] Theodorsen, T., General theory of aerodynamic instability and the mechanism of flutter, Report, NACA Technical Report No. 496, 1935.